Magnetic extraction of black hole rotational energy: Method and results of general relativistic magnetohydrodynamic simulations in Kerr space-time

Shinji Koide*
Department of Engineering, Toyama University, 3190 Gofuku, Toyama 930-8555, Japan
(Received 4 October 2002; published 19 May 2003)

We present the complete numerical method of general relativistic magnetohydrodynamic simulations in Kerr space-time, and then apply those techniques to the basic astrophysical problem of activity near a Kerr black hole immersed in a plasma with a large-scale magnetic field. Our numerical results show that a torsional Alfven wave is generated in the ergosphere of the Kerr black hole. This wave propagates outward along the magnetic field lines, extracting rotational energy from the plasma in the ergosphere. If the magnetic field is strong enough, the plasma energy in the ergosphere rapidly decreases and eventually becomes negative. When this negative energy plasma is swallowed by the black hole, the total energy of the black hole decreases, spinning it down. This energy extraction mechanism is similar to the ''Penrose process,'' in which the negative energy also plays an important role. The difference between the two is the force that causes the redistribution of the angular momentum (which is necessary to produce the negative energy). In the Penrose process, elementary particle interactions cause the redistribution, while in the present case it is performed by magnetic tension.

DOI: 10.1103/PhysRevD.67.104010 PACS number(s): 04.25.Dm, 04.70.−s, 52.30.Cv, 97.60.Lf

I. INTRODUCTION

Relativistic jets are often ejected from active objects in the universe. Superluminal motion, for example, has been observed not only from quasars and active galactic nuclei (AGNs) [1,2], but also from binary systems in our Galaxy such as GRS1915+105 and GRO J1655-40 [3,4]. Recently the most powerful explosions in the universe, gamma-ray bursts (GRBs), have been explained by extremely high Lorentz factor jets [5]. It is believed that such relativistic jets are formed near the black hole. Furthermore, because it is very difficult for any black hole to be formed with exactly zero angular momentum, it is believed that most black holes rotate. In fact, some measurements of black hole rotation suggest that most black holes rotate rapidly [6]. Two kinds of energy are available for generating a jet from a rotating (Kerr) black hole. One is the rotational energy of the accretion disk around the black hole and the other is the rotational energy of the Kerr black hole itself. In the latter case, it is the complex interaction between the rotating black hole and the strongly magnetized plasma around it that creates the relativistic jet engine. In this process, magnetic extraction of black hole rotational energy is the fundamental driver.

Extraction of Kerr black hole rotational energy was first proposed by Penrose [7]. He considered relativistic particle fission ($0 \rightarrow 1+2$) in the black hole's ergosphere. If the angular momentum of particle 2 is opposite to that of the black hole, and large enough, then the energy-at-infinity of particle 2 will be negative. And, because the total energy-at-infinity is conserved, the energy-at-infinity of particle 1 will be larger than that of the injected particle 0. When particle 2 (with the negative energy-at-infinity) is swallowed by the black hole and particle 1 is ejected, the total energy of the black hole decreases and the energy of the ejected particle outside the ergosphere increases. That is, rotational energy of the black hole has been extracted and imparted to particle 1. It should be noted that the propagation of material, energy, and information across the black hole horizon is only inward toward the black hole. That is, causality at the horizon is one-way. In the Penrose process, the falling of a negative energy-at-infinity particle through the horizon transports energy outward, extracting black hole rotational energy and obeying causality. Unfortunately, this process is not directly applicable to astrophysical jets for two reasons. In the Penrose process, the particle is accelerated in a direction perpendicular to the Kerr black hole rotation axis, creating a distribution of accelerated particles in the shape of a disk, not a jet. Furthermore, the mechanism requires frequent relativistic fission in the ergosphere in order to create the observed jets. This is not astrophysically plausible, as it requires the accretion of large amounts of fissionable material.

Blandford and Znajek investigated magnetospheres of Kerr black holes and derived a force-free, static solution for the electromagnetic field [8]. Their results show that electromagnetic energy is radiated from the black hole horizon directly, and the generated power can be large enough to explain observed astrophysical jets, if the magnetic field is strong enough. However, if we consider the dynamics of magnetic extraction of Kerr black hole rotational energy, direct energy radiation from the black hole appears to be inconsistent with causality at the horizon. A similar argument, but with respect to the flow critical points such as the magnetohydrodynamic (MHD) fast point, and not the horizon itself, was also presented by [9]. We discuss the Blandford-Znajek mechanism below, comparing it to our simulation results, and show that it indeed satisfies causality at the horizon.

To investigate the dynamics of electromagnetic extraction of black hole rotational energy, we have performed general relativistic magnetohydrodynamic (GRMHD) simulations of a rather simple system that involves a strong magnetic field, thin plasma, and a Kerr black hole [10]. The purpose of this

*Electronic address: koidesin@ecs.toyama-u.ac.jp

paper is to present the entire GRMHD numerical method in Kerr space-time and, as an application, to show the details of magnetic energy extraction from a Kerr black hole.

The reader will find the GRMHD equations in this paper are very similar to the non-relativistic MHD ones. Therefore, it is not that difficult to develop a GRMHD numerical code by modifying a non-relativistic MHD code. Non-relativistic MHD simulations have a long history, and various useful methods have been developed. Using the present form of the GRMHD equations in this paper, we are able to take advantage of much of this excellent previous work. The most crucial difference between GRMHD and non-relativistic MHD is the treatment of the displacement current. In non-relativistic MHD, the latter is negligible, while even in the special relativistic cases, it cannot be neglected. To calculate the displacement current, we must calculate the time evolution of the electric field or extrapolate the electric field from the previous variables. These are difficult to calculate without significant numerical error. Therefore, in GRMHD, accurate calculation of the electric current density **J** is difficult while in non-relativistic MHD **J** can be calculated easily. Here we use the conservation form of the GRMHD equations. In this case, we do not need to calculate the electric current and displacement current explicitly if the electric resistivity is negligible. This is much easier than using forms of the GRMHD equations that explicitly include the electric current density **J**.

The organization of this paper is as follows: in Sec. II we present the basic equations of GRMHD in Kerr space-time. In Sec. III, we illustrate the numerical method used in the simulations in this paper. The application of the numerical method, the detailed mechanism of magnetohydrodynamic extraction of Kerr black hole rotational energy, is shown in Sec. IV. A summary is briefly presented in Sec. V.

II. BASIC EQUATIONS

A. Four-dimensional form of GRMHD equations

GRMHD numerical methods are required in order to study the complex evolution of plasmas around a black hole. This method is based on the general relativistic formulation of the laws of particle number, energy-momentum, Maxwell equations, and Ohm's law with zero electrical resistance (*ideal MHD condition*) in curved space-time [11–15]. Here we will neglect radiation cooling effects, electric resistivity, plasma viscosity, and self-gravity in order to study the fundamentals of the interaction of Kerr black hole, magnetic field, and plasma. The space-time, $(x^0,x^1,x^2,x^3)=(ct,x^1,x^2,x^3)$ is described by a metric, $g_{\mu\nu}$, where the line element, ds is given by $(ds)^2=g_{\mu\nu}dx^\mu dx^\nu$. Here, Greek subscripts such as μ or ν run from 0 to 3, and c is the speed of light. The basic equations of GRMHD in four-dimensional space-time are

$$\nabla_\nu(\rho U^\nu)=\frac{1}{\sqrt{-\|g\|}}\frac{\partial}{\partial x^\nu}(\sqrt{-\|g\|}\rho U^\nu)=0, \tag{1}$$

$$\nabla_\nu T^{\mu\nu}=\frac{1}{\sqrt{-\|g\|}}\frac{\partial}{\partial x^\nu}(\sqrt{-\|g\|}T^{\mu\nu})+\Gamma^\mu_{\sigma\nu}T^{\sigma\nu}=0, \tag{2}$$

$$\partial_\mu F_{\nu\lambda}+\partial_\nu F_{\lambda\mu}+\partial_\lambda F_{\mu\nu}=0, \tag{3}$$

$$\nabla_\mu F^{\mu\nu}=-\mu_0 J^\nu, \tag{4}$$

where μ_0 is the magnetic permeability in a vacuum; $\|g\|$ is the determinant of the matrix with elements $g_{\mu\nu}$; $\Gamma^\lambda_{\mu\nu}\equiv\frac{1}{2}g^{\lambda\sigma}(-\partial g_{\mu\nu}/\partial x^\sigma+\partial g_{\nu\sigma}/\partial x^\mu+\partial g_{\sigma\mu}/\partial x^\nu)$ are the Christoffel symbols; ∇_ν is the covariant derivative [34]. Here, U^ν and $J^\nu=(c\rho_e,J^1,J^2,J^3)$ are the four-velocity and electric four-current density, respectively (ρ_e is the electric charge density); the general relativistic energy momentum tensor $T^{\mu\nu}$ is given by

$$T^{\mu\nu}=pg^{\mu\nu}+(e_{\rm int}+p)U^\mu U^\nu+F^\mu_\sigma F^{\nu\sigma}-\frac{1}{4}g^{\mu\nu}F^{\lambda\kappa}F_{\lambda\kappa}, \tag{5}$$

where $F^{\mu\nu}$ is the electromagnetic field-strength tensor, $F_{\mu\nu}=\partial_\mu A_\nu-\partial_\nu A_\mu$ and $A^\mu=(\phi_e/c,A^1,A^2,A^3)$ is four-vector potential (ϕ_e is the electro-static potential). The electric field E_i and the magnetic field B_i are given by $E_i=cF_{i0}$ $(i=1,2,3)$ and $B_1=F_{23}$, $B_2=F_{31}$, $B_3=F_{12}$, respectively. Scalar values, ρ, p, and $e_{\rm int}$ are proper mass density, proper pressure, and proper internal energy density, $e_{\rm int}=\rho c^2+p/(\Gamma-1)$, respectively, where Γ is the specific-heat ratio. In addition to the equations, we assume the infinite electric conductivity condition:

$$F_{\mu\nu}U^\nu=0. \tag{6}$$

Using this condition, Eqs. (1)–(3) close self-consistently. Equation (4) is used only to calculate the four-current density J^μ.

We assume that the off-diagonal spatial elements of the metric $g_{\mu\nu}$ vanish:

$$g_{ij}=0 \quad (i\neq j). \tag{7}$$

Here Roman indices (i,j) run from 1 to 3. If we write

$$g_{00}=-h_0^2, \quad g_{ii}=h_i^2, \tag{8}$$

$$g_{i0}=g_{0i}=-h_i^2\omega_i/c, \tag{9}$$

then the scale of a small element in space-time is given by

$$\begin{aligned}(ds)^2&=g_{\mu\nu}dx^\mu dx^\nu\\&=-h_0^2(cdt)^2+\sum_{i=1}^{3}[h_i^2(dx^i)^2-2h_i^2\omega_i dt dx^i].\end{aligned} \tag{10}$$

When we define the lapse function α and "shift velocity" (shift vector) β^i as

$$\alpha=\sqrt{h_0^2+\sum_{i=1}^{3}\left(\frac{h_i\omega_i}{c}\right)^2}, \tag{11}$$

$$\beta^i = \frac{h_i \omega_i}{c\alpha}, \tag{12}$$

the line element ds is written as

$$(ds)^2 = -\alpha^2 (cdt)^2 + \sum_{i=1}^{3} (h_i dx^i - c\beta^i \alpha dt)^2. \tag{13}$$

The determinant $\|g\|$ is given by $\sqrt{-\|g\|} = \alpha h_1 h_2 h_3$, and the contravariant metric is written explicitly as

$$g^{00} = -\frac{1}{\alpha^2}, \tag{14}$$

$$g^{i0} = g^{0i} = -\frac{1}{\alpha^2}\frac{\omega_i}{c}, \tag{15}$$

$$g^{ij} = \frac{1}{h_i h_j}(\delta^{ij} - \beta^i \beta^j), \tag{16}$$

where δ^{ij} is the Kronecker's δ symbol.

B. Kerr space-time

A Kerr black hole has two characteristic parameters: its mass M and its angular momentum J. We often use the rotation parameter $a = J/J_{\max}$, where $J_{\max} = GM^2/c$ is the angular momentum of a maximumly rotating black hole with mass M ($G = 6.67 \times 10^{-11}$ Nm^2/kg^2 is the gravitational constant). In the Boyer-Lindquist coordinates, $(x^0, x^1, x^2, x^3) = (ct, r, \theta, \phi)$, the metric of Kerr space-time is written as

$$h_0 = \sqrt{1 - \frac{2r_g r}{\Sigma}}, \quad h_1 = \sqrt{\frac{\Sigma}{\Delta}}, \quad h_2 = \sqrt{\Sigma}, \quad h_3 = \sqrt{\frac{A}{\Sigma}}\sin\theta, \tag{17}$$

$$\omega_1 = \omega_2 = 0, \quad \omega_3 = \frac{2cr_g^2 ar}{A}, \tag{18}$$

where $r_g \equiv GM/c^2$ is the gravitational radius, $\Delta = r^2 - 2r_g r + (ar_g)^2$, $\Sigma = r^2 + (ar_g)^2 \cos^2\theta$, and $A = \{r^2 + (ar_g)^2\}^2 - \Delta (ar_g)^2 \sin^2\theta$. Here, r, θ, and ϕ are the radial, colatitudinal, and azimuthal coordinates, respectively. In this metric, the lapse function is $\alpha = \sqrt{\Delta\Sigma/A}$. The radius of the event horizon is $r_H = r_g(1 + \sqrt{1 - a^2})$, which is found by setting $\alpha = 0$. We sometimes also use the Schwarzschild radius of the black hole, $r_S = 2GM/c^2 = 2r_g$ as a unit of length in this paper.

As it rotates, a black hole drags the space surrounding it. This is called the *frame-dragging* effect. Because of frame-dragging, there exists a special region just outside the hole, called the *ergosphere*, in which any matter, energy, and information must rotate in the same direction as the black hole rotation. The surface of the ergosphere is given by $h_0 = 0$, that is, $r = r_g(1 + \sqrt{1 - a^2\cos^2\theta})$. In the ergosphere, the shift velocity $c\beta^\phi$ is greater than the light speed. In the high rotation case ($a \sim 1$), the shape of the ergosphere surface is like that of an apple, with a cusp-like dimple at the top and bottom: at the pole it touches the horizon $r = r_H$, and on the equatorial plane, the radius is r_S. In the low rotation parameter case, $a < 0.8$, its shape is like an ellipsoid.

C. 3+1 formalism of the GRMHD equations

We present the 3+1 formalism of the GRMHD equations, derived from the four-dimensional expressions (1)–(4), and (6). In order to express observed physical quantities, we will use several different reference frames, as follows:

Laboratory frame

This is a global fixed frame, with the observer far from the black hole. For astrophysics, a better name might be the "observer-at-infinity" frame. For Kerr space-time, the coordinates of the frame are given by Boyer-Lindquist coordinates. In the laboratory frame we will write any contravariant vector as a^μ.

Local laboratory (LOLA) frame

While this is a very useful frame, there is no popular terminology for it. The "LOLA" frame is fixed to the laboratory frame, but an observer in this frame *sees* events locally only, that is, only those in the neighborhood of the observer. In this frame $(c\tilde{t}, \tilde{x}^1, \tilde{x}^2, \tilde{x}^3)$, the line element is written as

$$(ds)^2 = -(cd\tilde{t})^2 + \sum_i (d\tilde{x}^i - c\beta^i d\tilde{t})^2, \tag{19}$$

where $cd\tilde{t} = \alpha cdt$, $d\tilde{x}^i = h_i dx^i$. Therefore, a covariant vector measured in the "LOLA" frame is related to a^μ as

$$\tilde{a}^0 = \alpha a^0, \quad \tilde{a}^i = h_i a^i. \tag{20}$$

A covariant vector is expressed in the "LOLA" frame as

$$\tilde{a}_0 = \frac{1}{\alpha} a_0, \quad \tilde{a}_i = \frac{1}{h_i} a_i. \tag{21}$$

Fiducial observer (FIDO) frame

This is a locally inertial frame. Using the coordinates of the frame $(c\hat{t}, \hat{x}^1, \hat{x}^2, \hat{x}^3)$, the line element is

$$(ds)^2 = -(cd\hat{t})^2 + \sum_i (d\hat{x}^i)^2, \tag{22}$$

where $cd\hat{t} = cd\tilde{t}$, $d\hat{x}^i = d\tilde{x}^i - \beta^i cd\tilde{t}$. This is the same metric as that of Minkowski space-time. A contravariant vector $\hat{a}^\mu$ in the "FIDO" frame is

$$\hat{a}^0 = \tilde{a}^0, \quad \hat{a}^i = \tilde{a}^i - \tilde{a}^0 \beta^i \tag{23}$$

and the covariant vector $\hat{a}_\mu$ is

$$\hat{a}_0 = \tilde{a}_0 + \sum_i \beta^i \tilde{a}_i, \quad \hat{a}_i = \tilde{a}_i. \tag{24}$$

Note that, because the metric is Minkowskian, $\hat{a}^0 = -\hat{a}_0$ and $\hat{a}^i = \hat{a}_i$.

Comoving frame

An observer in this frame *rides on* the gas or the plasma and sees events locally. Quantities observed in this frame are often called *proper* values because they depend only on the nature of the gas or plasma itself. Any scalar quantity, such as pressure or density, is measured in this frame.

The components of vectors and tensors measured in the ''LOLA'' frame are given by Eqs. (20) and (21). To transform any tensor $q^{\mu\nu}$ we can simply consider the product of vectors like $a^\mu b^\nu$. Here, we denote these components with tilde. We find

$$\tilde{\gamma}=\alpha U^0, \tag{25}$$

$$\tilde{v}^i=\frac{h_i}{\tilde{\gamma}}cU^i, \tag{26}$$

$$\tilde{T}^{00}=\alpha^2 T^{00}, \tag{27}$$

$$\tilde{P}^i=\frac{1}{c}\tilde{T}^{i0}=\frac{\alpha h_i}{c}T^{i0}=\frac{\alpha h_i}{c}T^{0i}, \tag{28}$$

$$\tilde{T}^{ij}=h_i h_j T^{ij}, \tag{29}$$

$$\tilde{F}_{0i}=-\tilde{F}_{i0}=\frac{1}{\alpha h_i}F_{0i}, \tag{30}$$

$$\tilde{F}_{ij}=-\tilde{F}_{ij}=\frac{1}{h_i h_j}F_{ij}, \tag{31}$$

$$\tilde{\rho}_{\rm e}=\frac{\tilde{J}^0}{c}=\frac{1}{c}\alpha J^0, \tag{32}$$

$$\tilde{J}^i=h_i J^i. \tag{33}$$

We usually will use physical variables that are measured in the FIDO frame, which, using Eqs. (23) and (24), are given by

$$\hat{\gamma}=\tilde{\gamma}, \tag{34}$$

$$D=\hat{\gamma}\rho, \tag{35}$$

$$\hat{v}^i=\tilde{v}^i-c\beta^i, \tag{36}$$

$$\epsilon+Dc^2=\hat{T}^{00}=\tilde{T}^{00}, \tag{37}$$

$$\hat{P}^i=\frac{1}{c}\hat{T}^{i0}=\tilde{P}^i-\frac{1}{c}\beta^i\tilde{T}^{00}=\tilde{P}^i-\frac{\beta^i}{c}(\epsilon+Dc^2), \tag{38}$$

$$\hat{T}^{ij}=\tilde{T}^{ij}-\beta^i\tilde{T}^{0j}-\beta^j\tilde{T}^{i0}+\beta^i\beta^j\tilde{T}^{00}, \tag{39}$$

$$\hat{F}_{i0}=-\hat{F}_{0i}=\tilde{F}_{i0}+\sum_j \beta^j\tilde{F}_{ij}, \tag{40}$$

$$\hat{F}_{ij}=\tilde{F}_{ij}, \tag{41}$$

$$\hat{\rho}_{\rm e}=\tilde{\rho}_{\rm e}, \tag{42}$$

$$\hat{J}^i=\tilde{J}^i-\hat{\rho}_{\rm e}c\beta^i, \tag{43}$$

where $\hat{\gamma}$ is Lorentz factor; $\hat{v}^i$ is three-velocity; ϵ is energy density; and $\hat{P}^i$ is momentum density. We usually will write $\gamma=\hat{\gamma}$ and $\rho_{\rm e}=\hat{\rho}_{\rm e}$, omitting the hat.

The relationship between the variables measured in the FIDO frame is the same as that of special relativistic MHD [16,17]. Here, we summarize the relation

$$D=\gamma\rho, \tag{44}$$

$$\gamma=\frac{1}{\sqrt{1-\sum_{i=1}^{3}(\hat{v}^i/c)^2}}, \tag{45}$$

$$\hat{P}^i=\frac{1}{c^2}\mathfrak{h}\gamma^2\hat{v}^i+\frac{1}{c^2}(\hat{\mathbf{E}}\times\hat{\mathbf{B}})_i, \tag{46}$$

$$\hat{T}^{ij}=p\,\delta^{ij}+\frac{\mathfrak{h}}{c^2}\gamma^2\hat{v}^i\hat{v}^j+\left(\frac{\hat{B}^2}{2}+\frac{\hat{E}^2}{2c^2}\right)\delta^{ij}-\hat{B}_i\hat{B}_j-\frac{\hat{E}_i\hat{E}_j}{c^2}, \tag{47}$$

$$\epsilon=\mathfrak{h}\gamma^2-p-Dc^2+\frac{\hat{B}^2}{2}+\frac{\hat{E}^2}{2c^2}, \tag{48}$$

where $\mathfrak{h}$ is the relativistic enthalpy density, $\mathfrak{h}=\rho c^2+\Gamma p/(\Gamma-1)=e_{\rm int}+p$. Here, the magnetic field $\hat{\mathbf{B}}$ and the electric field $\hat{\mathbf{E}}$ are defined as

$$\hat{B}_i=\sum_{j,k}\frac{1}{2}\epsilon^{ijk}\hat{F}_{jk}, \tag{49}$$

$$\hat{E}_i=c\hat{F}_{i0}. \tag{50}$$

The following relations hold:

$$\hat{B}_i=\tilde{B}_i, \tag{51}$$

$$\hat{E}_i=\tilde{E}_i+\sum_{j,k}\epsilon^{ijk}c\beta^j\tilde{B}_k, \tag{52}$$

where

$$\tilde{B}_i=\sum_{j,k}\frac{1}{2}\epsilon^{ijk}\tilde{F}_{jk}, \tag{53}$$

$$\tilde{E}_i=c\tilde{F}_{i0}. \tag{54}$$

Using FIDO variables, we derive the following set of equations from the general relativistic conservation laws governing the plasma and from Maxwell equations (1)–(4) and (6):

$$\frac{\partial D}{\partial t}=-\frac{1}{h_1h_2h_3}\sum_i\frac{\partial}{\partial x^i}\left[\frac{\alpha h_1h_2h_3}{h_i}D(\hat{v}^i+c\beta^i)\right], \quad (55)$$

$$\frac{\partial \hat{P}^i}{\partial t}=-\frac{1}{h_1h_2h_3}\sum_j\frac{\partial}{\partial x^j}\left[\frac{\alpha h_1h_2h_3}{h_j}(\hat{T}^{ij}+c\beta^j\hat{P}^i)\right]$$
$$-(\epsilon+Dc^2)\frac{1}{h_i}\frac{\partial\alpha}{\partial x^i}+\alpha f^i_{\rm curv}-\sum_j\hat{P}^j\sigma_{ji}, \quad (56)$$

$$\frac{\partial\epsilon}{\partial t}=-\frac{1}{h_1h_2h_3}\sum_i\frac{\partial}{\partial x^i}\left[\frac{\alpha h_1h_2h_3}{h_i}c^2\left(\hat{P}^i-D\hat{v}^i+\frac{\beta^i}{c}\epsilon\right)\right]$$
$$-\sum_i c^2\hat{P}^i\frac{1}{h_i}\frac{\partial\alpha}{\partial x^i}-\sum_{i,j}\hat{T}^{ij}\sigma_{ji}, \quad (57)$$

$$\hat{E}_i=-\sum_{j,k}\epsilon_{ijk}\hat{v}^j\hat{B}_k, \quad (58)$$

$$\frac{\partial\hat{B}_i}{\partial t}=\frac{-h_i}{h_1h_2h_3}\sum_{j,k}\epsilon^{ijk}\frac{\partial}{\partial x^j}\left[\alpha h_k\left(\hat{E}_k-\sum_{l,m}\epsilon^{klm}c\beta^l\hat{B}_m\right)\right], \quad (59)$$

$$\sum_i\frac{1}{h_1h_2h_3}\frac{\partial}{\partial x^i}\left(\frac{h_1h_2h_3}{h_i}\hat{B}_i\right)=0, \quad (60)$$

$$\rho_{\rm e}=\sum_i\frac{1}{c^2}\frac{1}{h_1h_2h_3}\frac{\partial}{\partial x^i}\left(\frac{h_1h_2h_3}{h_i}\hat{E}_i\right), \quad (61)$$

$$\alpha(\hat{J}^i+\rho_{\rm e}c\beta^i)+\frac{1}{c^2}\frac{\partial\hat{E}_i}{\partial t}=\sum_{j,k}\frac{h_i}{h_1h_2h_3}\epsilon^{ijk}\frac{\partial}{\partial x^j}\left[\alpha h_k\left(\hat{B}_k+\sum_{l,m}\epsilon_{klm}\beta^l\frac{\hat{E}_k}{c}\right)\right], \quad (62)$$

where $f^i_{\rm curv}\equiv\Sigma_j(G_{ij}\hat{T}^{ij}-G_{ji}\hat{T}^{jj})$, $G_{ij}\equiv-(1/h_ih_j)\times(\partial h_i/\partial x^j)$, and $\sigma_{ij}\equiv(h_i/h_j)(\partial\omega_i/\partial x^j)$. This form for the equation is called the *3+1 form*, because the derivatives with respect to time and space are separated completely [18].

Throughout this paper, we used normalized forms of the magnetic field **B** and electric field **E**, so that $B^2/2$ and $E^2/2c^2$ present the magnetic and electric field energy density, respectively. We also normalize the electric charge density $\rho_{\rm e}$ and the electric current density **J** so that the Lorentz force density is given by $\mathbf{f}_{\rm L}=\rho_{\rm e}\mathbf{E}+\mathbf{J}\times\mathbf{B}$. The normalized variables used here are related to variables in MKSA unit system (SI unit system) as follows:

$$\mathbf{B}=\frac{\mathbf{B}^*}{\sqrt{\mu_0}}, \quad \mathbf{E}=\frac{\mathbf{E}^*}{\sqrt{\mu_0}}, \quad (63)$$

$$\rho_{\rm e}=\sqrt{\mu_0}\rho_{\rm e}^*, \quad \mathbf{J}=\sqrt{\mu_0}\mathbf{J}^*, \quad (64)$$

where a quantity with an asterisk is in the MKSA unit system.

D. Vector form of the GRMHD equations

We introduce the derivatives of arbitrary three-vector fields $\hat{\mathbf{a}}$ and $\hat{\mathbf{b}}$ and an arbitrary scalar field $\hat{\phi}$ measured by the FIDO frame:

$$\hat{\nabla}\cdot\hat{\mathbf{a}}=\sum_i\frac{1}{h_1h_2h_3}\frac{\partial}{\partial x^i}\left(\frac{h_1h_2h_3}{h_i}\hat{a}^i\right), \quad (65)$$

$$(\hat{\nabla}\hat{\phi})_i=\frac{1}{h_i}\frac{\partial\hat{\phi}}{\partial x^i}, \quad (66)$$

$$(\hat{\nabla}\times\hat{\mathbf{a}})_i=\sum_{j,k}\frac{h_i}{h_1h_2h_3}\epsilon_{ijk}\frac{\partial}{\partial x^j}(h_k\hat{a}^k), \quad (67)$$

$$[(\hat{\mathbf{b}}\cdot\hat{\nabla})\hat{\mathbf{a}}]_i=\sum_j\left[\frac{\hat{b}^j}{h_j}\frac{\partial\hat{a}^i}{\partial x^j}-G_{ij}\hat{a}^j\hat{b}^i+G_{ji}\hat{a}^j\hat{b}^j\right]. \quad (68)$$

Using these definitions, most formulae of standard vector analysis can be used without modification except for the following:

$$(\hat{\nabla}\times\hat{\mathbf{a}})\times\hat{\mathbf{b}}=(\hat{\mathbf{b}}\cdot\hat{\nabla})\hat{\mathbf{a}}-(\hat{\nabla}\hat{\mathbf{a}})\cdot\hat{\mathbf{b}}+[\hat{\mathbf{a}},\hat{\mathbf{b}}], \quad (69)$$

where $[(\hat{\nabla}\hat{\mathbf{a}})\cdot\hat{\mathbf{b}}]_i\equiv\Sigma_j\frac{1}{h_i}\frac{\partial\hat{a}^j}{\partial x^i}\hat{b}^j$ and $[\hat{\mathbf{a}},\hat{\mathbf{b}}]_i\equiv\Sigma_j G_{ij}(\hat{a}^j\hat{b}^i-\hat{a}^i\hat{b}^j)$. Furthermore, in the case of the relation

$$\hat{\nabla}\times(\hat{\mathbf{a}}\times\hat{\mathbf{b}})=(\hat{\nabla}\cdot\hat{\mathbf{b}})\hat{\mathbf{a}}+(\hat{\mathbf{b}}\cdot\hat{\nabla})\hat{\mathbf{a}}-(\hat{\nabla}\cdot\hat{\mathbf{a}})\hat{\mathbf{b}}-(\hat{\mathbf{a}}\cdot\hat{\nabla})\hat{\mathbf{b}}, \quad (70)$$

we will find it more useful to employ the following form:

$$[\hat{\nabla}\times(\hat{\mathbf{a}}\times\hat{\mathbf{b}})]_i=(\hat{\nabla}\cdot\hat{\mathbf{b}})\hat{a}^i-(\hat{\nabla}\cdot\hat{\mathbf{a}})\hat{b}^i+\sum_j\frac{h_i}{h_j}\left[\hat{b}^j\frac{\partial}{\partial x^j}\left(\frac{\hat{a}^i}{h_i}\right)-\hat{a}^j\frac{\partial}{\partial x^j}\left(\frac{\hat{b}^i}{h_i}\right)\right]. \quad (71)$$

With the above derivatives of the three-vector and scalar fields, the equations of GRMHD (55)–(62) can be re-written in their FIDO vector form

$$\frac{\partial D}{\partial t}=-\hat{\nabla}\cdot[\alpha D(\hat{\mathbf{v}}+c\boldsymbol{\beta})], \quad (72)$$

$$\frac{\partial\hat{\mathbf{P}}}{\partial t}=-\hat{\nabla}\cdot[\alpha(\hat{\mathbf{T}}+c\boldsymbol{\beta}\hat{\mathbf{P}})]-(\epsilon+Dc^2)\hat{\nabla}\alpha+\alpha\mathbf{f}_{\rm curv}-\hat{\mathbf{P}}\cdot\boldsymbol{\sigma}, \quad (73)$$

$$\frac{\partial\epsilon}{\partial t}=-\hat{\nabla}\cdot[\alpha(c^2\hat{\mathbf{P}}-Dc^2\hat{\mathbf{v}}+\epsilon c\boldsymbol{\beta})]-(\hat{\nabla}\alpha)\cdot c^2\hat{\mathbf{P}}-\hat{T}:\boldsymbol{\sigma}, \quad (74)$$

$$\frac{\partial \hat{\mathbf{B}}}{\partial t} = -\hat{\nabla}\times[\alpha(\hat{\mathbf{E}} - c\boldsymbol{\beta}\times\hat{\mathbf{B}})], \tag{75}$$

$$\alpha(\hat{\mathbf{J}} + \hat{\rho}_e c\boldsymbol{\beta}) + \frac{1}{c^2}\frac{\partial \hat{\mathbf{E}}}{\partial t} = \hat{\nabla}\times\left[\alpha\left(\hat{\mathbf{B}} + \frac{1}{c}\boldsymbol{\beta}\times\hat{\mathbf{E}}\right)\right], \tag{76}$$

$$\hat{\nabla}\cdot\hat{\mathbf{B}} = 0, \tag{77}$$

$$\hat{\rho}_e = \frac{1}{c^2}\hat{\nabla}\cdot\hat{\mathbf{E}}, \tag{78}$$

$$\hat{\mathbf{E}} + \hat{\mathbf{v}}\times\hat{\mathbf{B}} = \mathbf{0}, \tag{79}$$

where $\boldsymbol{\beta}$ is three-vector with the components β_i, $\boldsymbol{\beta} = (\beta_1, \beta_2, \beta_3)$. These equations are very similar to the conservative form of the non-relativistic MHD equations except for the geometric factors and terms involving the lapse function α and the shift velocity $\boldsymbol{\beta}$. Note that $-c^2\hat{\nabla}\alpha$ corresponds to the gravitational force in the non-relativistic equations and that $c^2\alpha$ can be regarded as the (specific) gravitational potential. The term $\alpha\mathbf{f}_{\rm curv}$ contains the centrifugal force. The terms involving $\boldsymbol{\sigma}$ arise from the shear of the space dragging itself.

III. NUMERICAL METHOD

For our GRMHD simulations we use the *simplified total variation diminishing* (TVD) method, which was developed by Davis [19] for violent phenomena such as shocks (see Appendix D in [13]). This method is similar to the Lax-Wendroff method with the addition of a diffusion term. In the simplified method, in order to integrate the time-dependent conservation laws, we need only the maximum speed of waves, not each eigenvector or eigenvalue of the coefficient matrix of the linearized GRMHD equations.

During the evolution of the difference equations, we obtain only the quantities D, $\hat{\mathbf{P}}$, ϵ, and $\hat{\mathbf{B}}$ directly at each step. In order to proceed further, we must calculate the primitive variables γ, $\hat{\mathbf{v}}$, and p from the conserved quantities D, $\hat{\mathbf{P}}$, ϵ, and $\hat{\mathbf{B}}$ using Eqs. (44), (45), (46), and (48). To do this, we solve two nonlinear, simultaneous algebraic equations with unknown variables $x \equiv \gamma - 1$ and $y \equiv \gamma(\hat{\mathbf{v}}\cdot\hat{\mathbf{B}})/c^2$,

$$x(x+2)\left[\Gamma R x^2 + (2\Gamma R - d)x + \Gamma R - d + u + \frac{\Gamma}{2}y^2\right]^2 = (\Gamma x^2 + 2\Gamma x + 1)^2[f^2(x+1)^2 + 2\sigma y + 2\sigma x y + b^2 y^2], \tag{80}$$

$$\left[\Gamma(R - b^2)x^2 + (2\Gamma R - 2\Gamma b^2 - d)x + \Gamma R - d + u - b^2 + \frac{\Gamma}{2}y^2\right]y = \sigma(x+1)(\Gamma x^2 + 2\Gamma x + 1), \tag{81}$$

where $R = D + \epsilon/c^2$, $d = (\Gamma - 1)D$, $u = (1 - \Gamma/2)\hat{B}^2/c^2$, $f = \hat{P}/c$, $b = \hat{B}/c$, and $\sigma = \hat{\mathbf{B}}\cdot\hat{\mathbf{P}}/c^2$. Note that, in the absence of the magnetic field $\mathbf{B}$, Eq. (80) reduces to the well-known relativistic hydrodynamic one, derived by Duncan and Hughes [20], and Eq. (81) becomes a trivial equation. These algebraic equations are solved at each cell using a 2-variable Newton-Raphson iteration method. The primitive variables then are calculated easily from x, y, D, $\hat{\mathbf{P}}$, ϵ, and $\hat{\mathbf{B}}$, using

$$\gamma = 1 + x, \tag{82}$$

$$p = \frac{(\Gamma - 1)[\epsilon - xDc^2 - (2 - 1/\gamma^2)B^2/2 + (cy/\gamma)^2/2]}{[\Gamma x(x+2) + 1]}, \tag{83}$$

$$\hat{\mathbf{v}} = \frac{\mathbf{P} + (y/\gamma)\mathbf{B}}{D + \{\epsilon + p + B^2/2\gamma^2 + (cy/\gamma)^2/2\}/c^2}. \tag{84}$$

This method is identical to that used in special relativistic MHD simulations [16,17]. Our numerical code has been tested in both the special relativistic regime [16,17] and in the general relativistic regime [13], the latter using a Schwarzschild black hole. We also checked the code performance in a Kerr metric by computing circular orbits and their stability inside and outside of the last stable orbit [35].

IV. A SIMULATION OF MAGNETIC EXTRACTION OF ROTATIONAL ENERGY FROM A KERR BLACK HOLE

A. Initial and boundary conditions

To understand the basic physics of magnetic extraction of rotational energy from a black hole, we have used GRMHD simulations to investigate a simple system involving a large-scale magnetic field, thin plasma, and nearly maximally-rotating Kerr black hole with $a = 0.99995$. In this case, the black hole horizon radius is $r_{\rm H} = 0.505 r_{\rm S}$. The plasma around the hole is initialized with a uniform mass density ρ_0, low pressure $p_0 = 0.06\rho_0 c^2$, and a specific-heat ratio of $\Gamma = 5/3$. The initial momentum of the plasma is zero everywhere, and the initial magnetic field is uniform and strong. Its initial structure is given by the uniform and steady Wald solution [21] for a magnetic field in a vacuum. The electric field is given by the ideal MHD condition (79). The vector potential of the Wald solution is

$$A_\mu = \frac{B_0}{2}(g_{\mu 3} + 2ar_{\rm g}g_{\mu 0}), \tag{85}$$

where B_0 is a constant indicating the magnetic field strength. In Boyer-Lindquist coordinates, $(x^0, x^1, x^2, x^3) = (ct, r, \theta, \phi)$, this yields

$$\hat{B}_r = B_0\frac{\cos\theta}{\sqrt{A}}\left[\Delta + \frac{2r_{\rm g}r(r^4 - (ar_{\rm g})^4)}{\Sigma^2}\right], \tag{86}$$

$$\hat{B}_\theta = -B_0\sqrt{\frac{\Delta}{A}}\sin\theta\Bigg[r - r_g + \frac{r_g}{\Sigma^2}\{(r^2+(ar_g)^2)\Sigma + 2(ar_g)^2\cos^2\theta(r^2-(ar_g)^2)\}\Bigg]. \quad (87)$$

In the present simulation, we set as $B_0 = 5.77\sqrt{\rho_0 c^2}$. This is a magnetic-field-dominated case, with Alfven velocity, $v_A = B_0/[\rho_0 + \{\Gamma p_0/(\Gamma-1) + B_0^2\}/c^2]^{1/2} = 0.983c$ close to the speed of light [36].

We perform simulations in the region $0.51r_S \leqslant r \leqslant 20r_S$ and $0.01 \leqslant \theta \leqslant \pi/2$, with 211×71 mesh points. We use a uniform mesh in the coordinates $(\log r, \theta, \phi)$ and assume axisymmetry with respect to the z-axis and reflection symmetry with respect to the equatorial plane. The axisymmetric conditions on the z-axis ($\theta = 0, \pi$) are

$$\frac{\partial D}{\partial\theta} = 0, \quad \frac{\partial \hat{P}^r}{\partial\theta} = 0, \quad \hat{P}^\theta = 0, \quad \hat{P}^\phi = 0, \quad \frac{\partial \epsilon}{\partial\theta} = 0,$$

$$\frac{\partial \hat{B}_r}{\partial\theta} = 0, \quad \hat{B}_\theta = 0, \quad \hat{B}_\phi = 0,$$

and the reflection symmetry conditions on the equatorial plane ($\theta = \pi/2$) are given by

$$\frac{\partial D}{\partial\theta} = 0, \quad \frac{\partial \hat{P}^r}{\partial\theta} = 0, \quad \hat{P}^\theta = 0, \quad \frac{\partial \hat{P}^\phi}{\partial\theta} = 0, \quad \frac{\partial \epsilon}{\partial\theta} = 0,$$

$$\hat{B}_r = 0, \quad \frac{\partial \hat{B}_\theta}{\partial\theta} = 0, \quad \hat{B}_\phi = 0.$$

A radiative boundary condition is employed at $r = 0.51r_S$ and $r = 20r_S$:

$$u_0^{n+1} = u_0^n + u_1^{n+1} - u_1^n, \quad (88)$$

where u is any conserved density (D, **P**, ϵ, **B**). The superscripts n and $n+1$ indicate the time step numbers, and the subscripts 0 and 1 show the boundary and its neighboring mesh points, respectively.

B. Time evolution and three-dimensional view of the system

Figure 1 shows the time evolution of this system of large-scale magnetic field, thin plasma, and Kerr black hole. Hereafter, we will discuss the physics in the Boyer-Lindquist coordinates (the laboratory frame) except when noted. At $t = \tau_S = r_S/c$, the plasma begins to fall rapidly toward the black hole, and the azimuthal component of the magnetic field also begins to increase due to the azimuthal twisting of the magnetic field lines (Fig. 1b). In the ergosphere, the plasma rotates in the same direction as the black hole due to the frame dragging effect. The magnetic field lines then are twisted azimuthally in the direction of the black hole rotation by the differential rotation of the plasma. This effect is similar, in a broad sense, to the the dynamo effect called Ω effect of geomagnetic dynamo theory and therefore called the

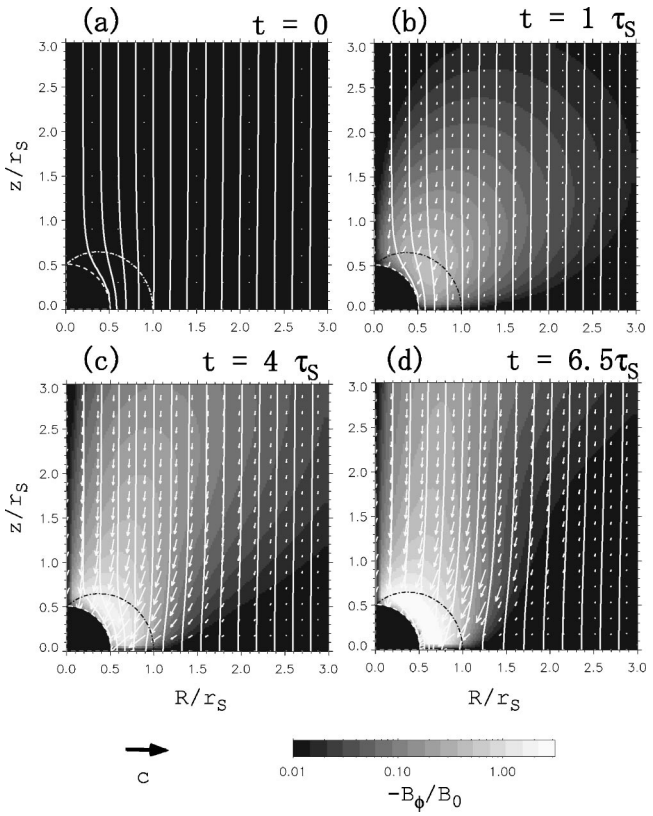

FIG. 1. Time evolution of a simple system of large-scale strong magnetic field, thin plasma, and a Kerr black hole in the region $0 \leqslant R \equiv r\sin\theta \leqslant 3r_S$ and $0 \leqslant z \equiv r\cos\theta \leqslant 3r_S$. The gray-scale portion shows the value of $-B_\phi/B_0$, and solid lines are poloidal magnetic field lines (flux surfaces). The arrows show the poloidal component of the plasma velocity $\hat{\mathbf{v}}$ as observed in the FIDO frame. The black quarter-circle at the origin indicates the event horizon of the black hole. The dashed line shows the inner boundary of the calculation region at $r = 1.01r_H$. The dot-dashed lines show the boundary of the ergosphere.

''frame-dragging dynamo'' (or ''frame-dragging Ω effect'') [22,23]. At $t = 6.53\tau_S$, this process has amplified the magnetic field to a value that is three times larger than the initial magnetic field strength in the ergosphere (Fig. 1d). The twist of the magnetic field lines propagates outward along the magnetic field lines against the infalling plasma flow as a torsional Alfven wave (Figs. 1b, 1c, and 1d; see the expansion of the gray-white region). We call this wave propagation region ''Alfven wave region.'' The production and propagation of a torsional Alfven wave also can occur in an accretion disk in Kepler orbital rotation about a normal star if there is a large-scale magnetic field [24–29]. The difference between Alfven waves from an ergosphere and a magnetized accretion disk is that the former are caused by the frame-dragging effect, while the latter are due to the rotation of the disk. In the disk case, if the rotation stops, no Alfven wave is produced. However, independent of the state of the plasma, an Alfven wave will be emitted from the ergosphere if the black hole is rotating.

To demonstrate this result more intuitively, we show in three-dimensions the magnetospheric structure around the

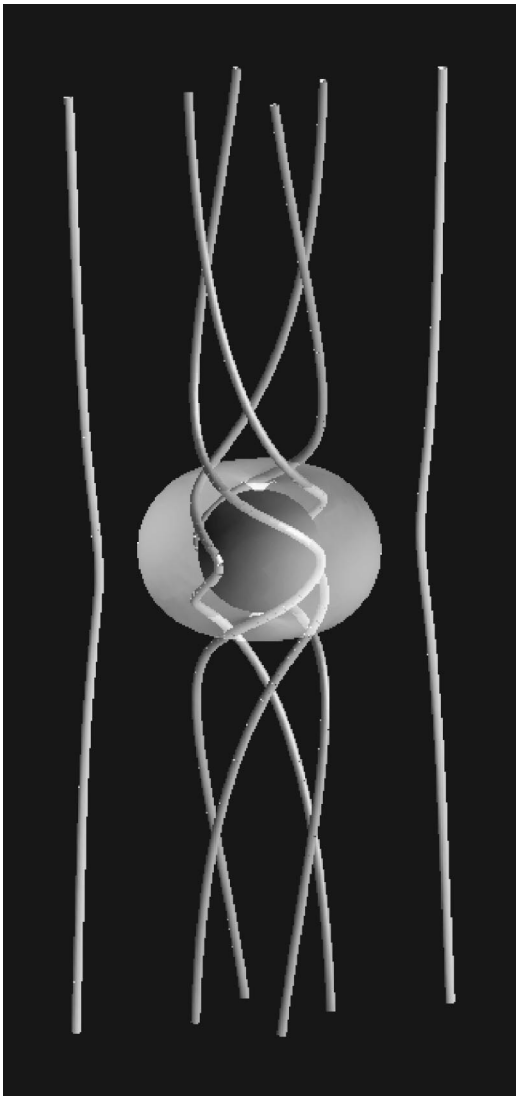

FIG. 2. Three-dimensional graphic of magnetic field lines around a Kerr black hole at $t=6.53\tau_S$. The black sphere at the center depicts the black hole. The transparent surface shaped like an apple outside the black hole is that of the ergosphere. The tubes show the magnetic field lines. Four of these penetrate into the ergosphere and the two others do not.

Kerr black hole at $t=6.53\tau_S$ (Fig. 2). The magnetic field lines are drawn so that they are parallel to the magnetic field observed in the laboratory frame at each point. At this time, the black hole has rotated one cycle since the beginning of the simulation. The magnetic field lines are slightly bent toward the black hole by the infalling plasma. Those field lines that penetrate the ergosphere surface are twisted strongly azimuthally in the same direction as the black hole rotation, which those that do not penetrate it are twisted only weakly. The magnetic tension of the bent magnetic field decelerates the plasma in the ergosphere near the equatorial plane, imparting an angular momentum that is opposite to that of the black hole. The importance of this effect is shown later.

C. Energy transport in the system

Next we shall discuss the details of energy transport in our example simulation. The basis theory and sense of energy transport near a Kerr black hole are summarized in the Appendix. Figure 3 shows the energy-at-infinity density e^∞ and the energy flux density **S** at $t=6.53\tau_S$. The figure shows that there is a net energy flux out of the ergosphere along the magnetic field lines. Integrating the energy flux density **S** over the surface of a cylinder $R\equiv r\sin\theta\leqslant 0.8r_S$, $-r_S\leqslant z\equiv r\cos\theta\leqslant r_S$, we found the net power is $L_{\rm tot}=0.186B_0^2r_S^2c/\mu_0$. This energy flux is so large that the total energy-at-infinity density e^∞ of the material and the field in the ergosphere decreases quickly and has become decidedly negative by $t=6.53\tau_S$. The dotted lines show positive energy-at-infinity contours and solid lines show non-positive (zero or negative) values. When this net negative energy-at-infinity is swallowed by the black hole, the net energy (total mass) of the black hole decreases. Energy of the Kerr black hole, therefore, has been converted to electromagnetic field energy of the Alfven wave. We call the region where the plasma with the negative energy-at-infinity accretes toward the black hole the ''negative energy falling region.''

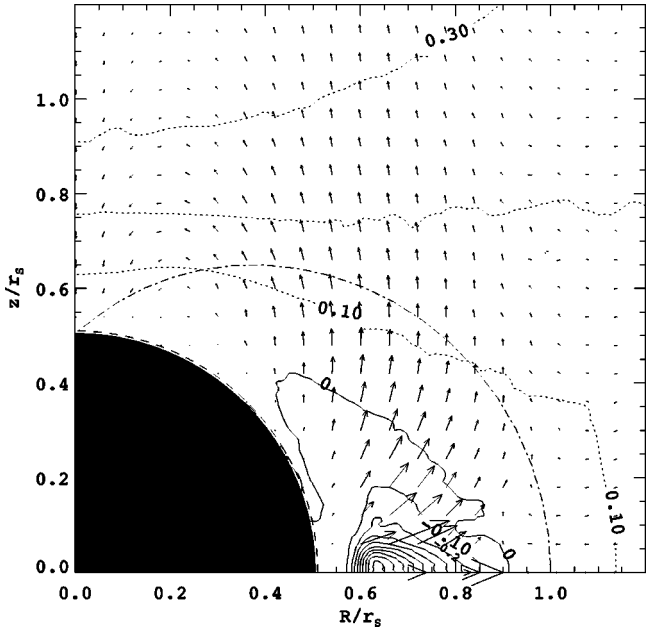

FIG. 3. The energy-at-infinity density e^∞ and the energy flux density **S** at $t=6.53\tau_S$. The dotted lines show the positive value of e^∞ and the solid lines show the non-positive (zero or negative) value. The arrows show the energy flux density **S**. The black region and dashed and dot-dashed lines are the same as Fig. 1.

Note that, in Boyer-Lindquist coordinates, any material, energy, and information outside the black hole horizon can not cross the horizon because of the time dilation effects there. However, in Fig. 3 it appears that the negative energy-at-infinity region extends all the way to the horizon. This is an artifact of the extrapolation of variables from the calculation boundary at $r=0.51r_S$. Physically this means only that the negative energy-at-infinity region reaches to the calculation boundary (the ''stretched'' horizon in our computation). Note also that the energy-at-infinity

$$E^\infty=\int_{r_H<r<\infty} e^\infty h_1h_2h_3dx^2dx^2dx^3 \qquad (89)$$

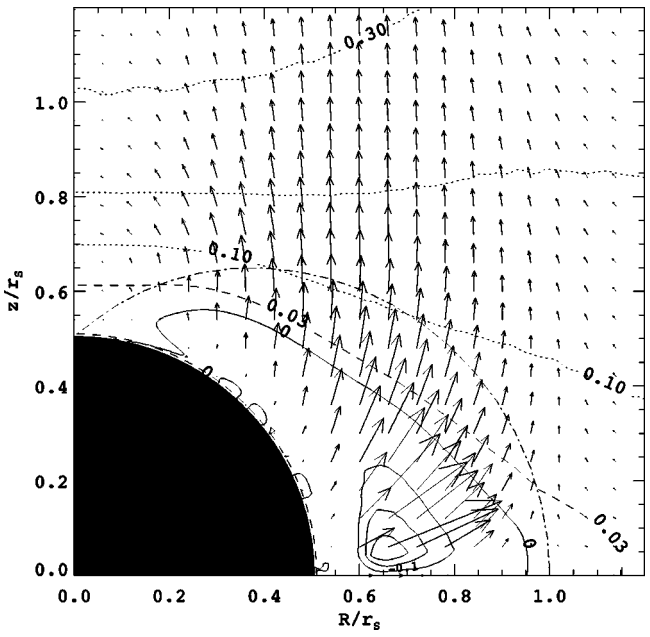

FIG. 4. Similar to Fig. 3, but for the electromagnetic energy-at-infinity density $e^{\infty}_{\rm EM}$ and the electromagnetic energy flux density $\mathbf{S}_{\rm EM}$.

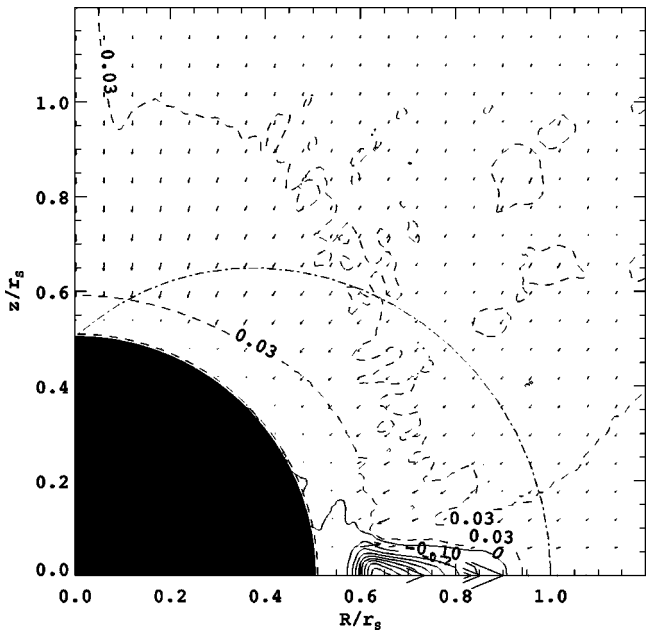

FIG. 5. Similar to Fig. 3, but for the hydrodynamic energy-at-infinity density $e^{\infty}_{\rm hyd}$ and the hydrodynamic energy flux density $\mathbf{S}_{\rm hyd}$.

is conserved, because energy transport across the horizon is zero due to the time dilation in the Boyer-Lindquist coordinates. We check this conserved quantity by integrating

$$E^{\infty}_{\rm N}=\int_{1.01r_{\rm H}<r<20r_{\rm S}} e^{\infty}h_1h_2h_3dx^2dx^2dx^3$$

and found that it is constant within the 0.2% accuracy. To compute the negative energy swallowed by the black hole directly, we should use other coordinates such as the Kerr-Schild coordinates [30].

Figures 4 and 5 show, respectively, the electromagnetic and hydrodynamic components of energy transport at $t=6.53\ \tau_{\rm S}$. The hydrodynamic energy flux density $\mathbf{S}_{\rm hyd}$ in Fig. 5 is directed toward the black hole everywhere except in the negative $e^{\infty}_{\rm hyd}$ region near the ergospheric equator. The absolute value of the outward hydrodynamic energy flux density on the equator $\mathbf{S}$ is much larger than that of the inward hydrodynamic energy flux, indicating that most of the hydrodynamic power emanates from the vicinity of the horizon (see also Fig. 3). Furthermore, the hydrodynamic energy there is more negative than even the electromagnetic energy, so when the plasma crosses the horizon, it is the negative *hydrodynamic* energy-at-infinity that will dominate the energy extraction. Such energy transport occurs in the negative energy falling region. On the other hand, Fig. 4 shows that the energy flux *from the ergosphere* is dominated by the *electromagnetic*, not the hydrodynamic, component. That is, there exists another region in the ergosphere, called the Alfven wave region (at $r\gtrsim 0.6r_{\rm S}$), where the outward electromagnetic energy flux is found. These two regions play different roles: plasma with negative hydrodynamic energy-at-infinity directly extracts the rotational energy of the black hole through the horizon, while electromagnetic energy is transported outward by the torsional Alfven wave produced in the ergosphere. Between the Alfven wave region and the negative energy falling region, hydrodynamic energy is transformed into magnetic energy. This is accomplished via magnetic tension in the ergospheric equatorial plane (Fig. 2). This tension accelerates the plasma in the ergosphere in a direction opposite to the rotation of the black hole. The shear converts hydrodynamic energy of the plasma into electromagnetic free energy by increasing the strength of the azimuthal magnetic field component. This is the frame-dragging dynamo effect, so we call the region in between the negative energy falling region and the Alfven wave region the ''frame-dragging dynamo region.''

Using the same method we used to calculate $L_{\rm tot}$, we find that the power of the Alfven wave emanating from the ergosphere is $L_{\rm EM}=0.259B_0^2r_{\rm S}^2c/\mu_0$. Punsly and Coroniti estimated the electromagnetic power from their ergosphere wind to be comparable to that coming directly from the rapidly rotating black hole horizon due to the Blandford-Znajek mechanism [8,9]: $L_{\rm BZ}\sim(\pi/4)a^2B_0^2r_{\rm H}^2c/\mu_0$. This yields $L_{\rm BZ}\sim 0.2B_0^2r_{\rm S}^2c/\mu_0$ for the present simulation which is almost the same as the value we obtained from our numerical simulation. A better expression for the power is $L_{\rm EM}=(\pi/4)(a^2c/v_{\rm A})B_0^2r_{\rm H}^2c/\mu_0$, which is valid when the inertia of the plasma is significant, the Alfven velocity is small compared to the speed of light, where the effects of plasma infall is neglected. On the other hand, hydrodynamic energy is transported *toward* the black hole with a rate of only $L_{\rm hyd}\sim -0.073B_0^2r_{\rm S}^2c/\mu_0$, which includes the inflow of the rest mass energy.

D. Angular momentum redistribution

Our numerical results show that rotational energy of a black hole can be causally extracted by a strong, large-scale

magnetic field if and only if negative energies-at-infinity occur within the ergosphere. The energy-at-infinity density is written as

$$e^{\infty} = \alpha e + \omega_{\phi} l \tag{90}$$

where $e \equiv \epsilon + Dc^2$ is the total energy density observed in the FIDO frame, and l is the angular momentum density [Eqs. (A4) and (A13) in the Appendix]. The lapse function α and e are always positive. So, to obtain negative energies-at-infinity, l must be negative and smaller than $-\alpha e/\omega_{\phi}$ (when ω_{ϕ} is positive). Now, because of time dilation at the horizon, the *total* angular momentum outside the horizon

$$L = \int_{r_{\rm H} < r < \infty} l h_1 h_2 h_3 dx^1 dx^2 dx^3 \tag{91}$$

must be conserved. Therefore, in order to obtain a sufficiently negative local angular momentum density l, there must be a redistribution of angular momentum in the ergosphere. We checked the expected conservation of L by integrating l and $|l|$ over the calculation volume and found that

$$\frac{\left| \int_{1.01 r_{\rm H} \leqslant r \leqslant 20 r_{\rm S}} l h_1 h_2 h_3 dx^1 dx^2 dx^3 \right|}{\int_{1.01 r_{\rm H} \leqslant r \leqslant 20 r_{\rm S}} |l| h_1 h_2 h_3 dx^1 dx^2 dx^3} = 0.18$$

at $t = 6.53 \tau_{\rm S}$. This means that most of the positive and negative angular momenta cancel to better than 20%.

Figure 6 shows the total angular momentum density l and its transport flux density $\mathbf{M}$ at $t = 6.53 \tau_{\rm S}$. The flux density shows that angular momentum is transported outward (see the Appendix). In the wide region around the ergosphere, the angular momentum density is negative, while in the outer region (around $R = 0.8 r_{\rm S}$, $z = 2.5 r_{\rm S}$) the angular momentum density is positive. The redistribution of angular momentum is caused by the electromagnetic field (see Fig. 7, the electromagnetic angular momentum transport flux density, $\mathbf{M}_{\rm EM}$), particularly by the magnetic tension. Note that the negative angular momentum l in the ergosphere is dominated by the hydrodynamic component (see $l_{\rm hyd}$ in Fig. 8). This is consistent with the negative energy-at-infinity being dominated by the hydrodynamic component, as noted earlier. Outside the ergosphere, the hydrodynamic angular momentum is negligible, and the positive angular momentum l is dominated by the electromagnetic component. This is also consistent with the energy transportation being due to the torsional Alfven wave.

E. Discussion

Energy transport in the entire system, and the ultimate extraction of black hole rotational energy by a large-scale magnetic field, can be summarized as follows. Because of the outward propagation of the electromagnetic free energy (against the plasma inflow) in the Alfven wave region, the energy-at-infinity in the ergosphere decreases to negative values. As material with negative energy-at-infinity can never escape the ergosphere, it subsequently will cross the horizon (if we observe in the Kerr-Schild coordinates). When negative energy plasma is swallowed by the black hole, the net energy of the Kerr black hole decreases. Here, the infall of gas with negative energy-at-infinity plays an essential role in operating a causally-correct, black hole energy extraction mechanism. To obtain negative energy-at-infinity in the gas, a relativistic angular momentum in the ergosphere *opposite* to the black hole's angular momentum is necessary. And, because the total angular momentum must be conserved, a

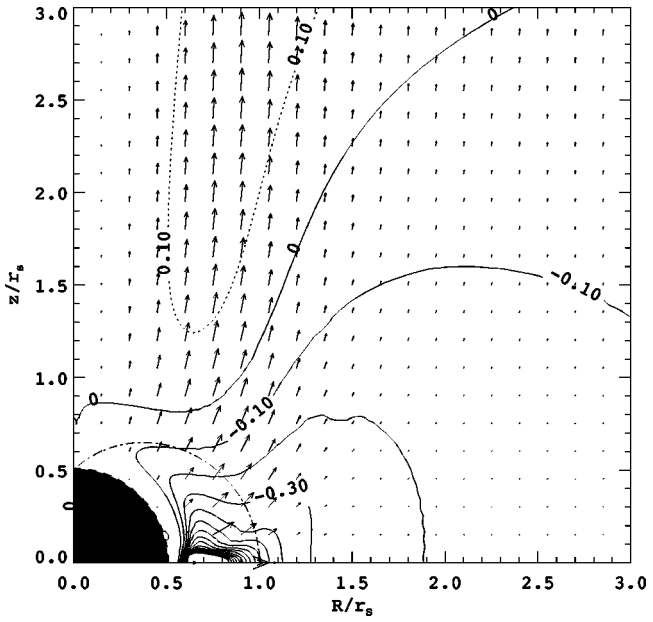

FIG. 6. Similar to Fig. 3, but for the angular momentum density l and the angular momentum flux density $\mathbf{M}$.

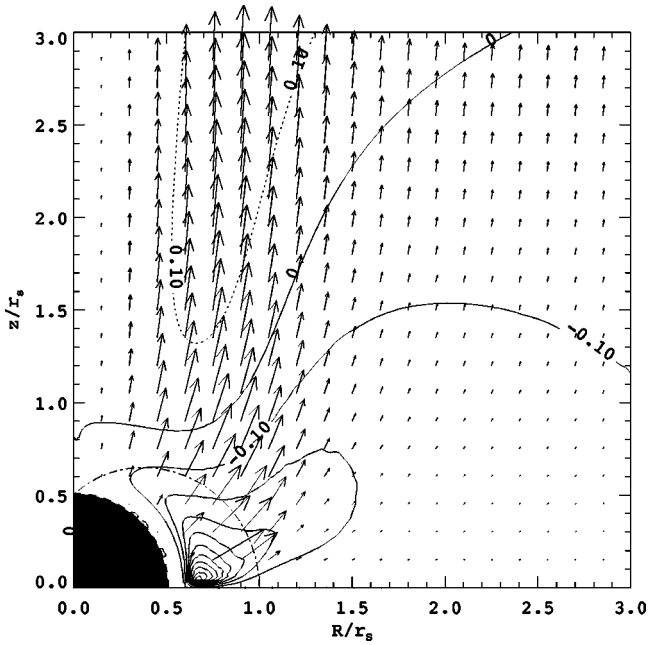

FIG. 7. Similar to Fig. 3, but for the electromagnetic angular momentum density $l_{\rm EM}$ and the electromagnetic angular momentum flux density $\mathbf{M}_{\rm EM}$.

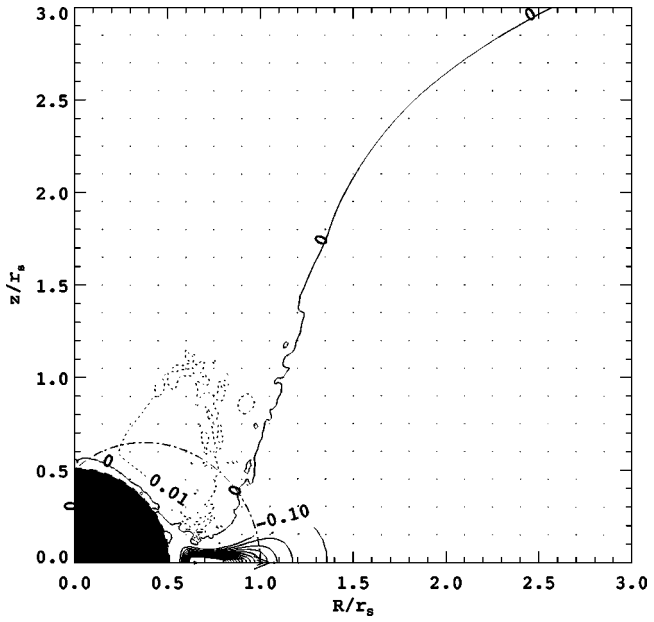

FIG. 8. Similar to Fig. 3, but for the hydrodynamic angular momentum density $l_{\rm hyd}$ and the hydrodynamic angular momentum flux density $\mathbf{M}_{\rm hyd}$.

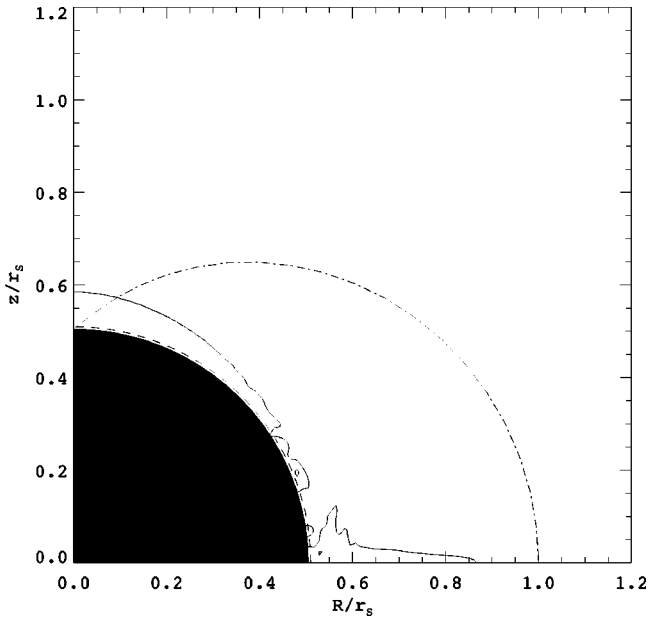

FIG. 9. The Alfven surface ($\hat{v}_{\rm f}^{\rm p}=\hat{v}_{\rm A}^{\rm p}$), indicated by the solid line. The black region and dashed and dot-dashed lines are the same as Fig. 1.

redistribution of the angular momentum is required. In the classic Penrose process an elementary particle reaction redistributes the angular momentum of particles into orbits with negative energy-at-infinity. Our simulation shows that the large-scale, strong magnetic field plays a role similar to particle scattering. Therefore, we call this magnetic extraction mechanism of black hole rotation energy the ''magnetohydrodynamic (MHD) Penrose process'' [31–33].

In order to propagate the Alfven wave outward against the infalling plasma, the Alfven velocity should be larger than the infall poloidal velocity of the plasma, $\hat{v}_{\rm f}^{\rm p}\equiv\sqrt{\hat{v}_r^2+\hat{v}_\theta^2}<\hat{v}_{\rm A}^{\rm p}\equiv\sqrt{(\hat{B}_r^2+\hat{B}_\theta^2)/[\rho+\{\Gamma p/(\Gamma-1)+B^2\}/c^2]}$. This condition delineates the volume we call the Alfven wave region, and the boundary of that region, where $\hat{v}_{\rm f}^{\rm p}=\hat{v}_{\rm A}^{\rm p}$, is called the Alfven surface. To extract the energy of the black hole, the Alfven wave region must be located in the ergosphere. The same result was found in the steady-state theory [31]. Figure 9 shows the Alfven surface at $t=6.53\tau_{\rm S}$. It is clearly located very near the horizon, and the figure shows that, even in the ergosphere, the Alfven wave propagates outwardly against the plasma falling along the magnetic field lines. Note that some parts of the Alfven surface appear to actually touch the horizon. This again is an artifact due to the extrapolation of the physical variables from the calculation boundary. It means only that the Alfven surface is located between the horizon at $r_{\rm H}=0.505r_{\rm S}$ and the calculation boundary at $r=0.510r_{\rm S}$. In the extremely strong magnetic field (or extremely low inertia plasma) case, the Alfven velocity approaches the speed of light: $\hat{v}_{\rm A}\to c(B^2/\rho c^2\to\infty)$. Because the plasma infall velocity is smaller than light speed ($\hat{v}_{\rm f}<c$), the condition $\hat{v}_{\rm f}<\hat{v}_{\rm A}$ is satisfied everywhere except at the horizon. In this case, the Alfven wave region spreads all around the Kerr black hole except at the horizon. This extremely strong magnetic field case corresponds to the force-free solution of Blandford-Znajek mechanism [8]. In this situation the critical surface, like Alfven and fast surfaces, is located at the horizon.

We now will show the existence of a negative energy falling region in the force-free solution of [8]. Here we do not need to consider the frame-dragging dynamo region because we can neglect the hydrodynamic energy-at-infinity in the solution. When the system is in a steady state, and axisymmetric with respect to the z-axis, the angular velocity of the magnetic field lines $\Omega_{\rm F}$ is constant along the magnetic flux surfaces [8]. The velocity of field lines in the FIDO frame is

$$\hat{\mathbf{v}}_{\rm F}=\frac{h_\phi}{\alpha}(\Omega_{\rm F}-\omega_\phi)\hat{\phi}, \tag{92}$$

and the electric field is

$$\hat{\mathbf{E}}=-\hat{\mathbf{v}}_{\rm F}\times\hat{\mathbf{B}}^{\rm p}, \tag{93}$$

where $\hat{\phi}$ is the azimuthal unit vector and $\hat{\mathbf{B}}^{\rm p}$ is the poloidal magnetic field [18]. The electromagnetic energy-at-infinity [Eq. (A9) in the Appendix] is

$$\begin{aligned} e_{\rm EM}^{\infty}&=\frac{\alpha}{2}\left[(\hat{B}^{\rm p})^2\left\{1+\left(\frac{\hat{v}_{\rm F}^{\phi}}{c}\right)^2+2\frac{\hat{v}_{\rm F}^{\phi}v_{\rm H}^{\phi}}{c^2}\right\}+\hat{B}_\phi^2\right] \\ &=\frac{\alpha}{2}(\hat{B}^{\rm p})^2\left[\left(\frac{\hat{v}_{\rm F}^{\phi}+v_{\rm H}^{\phi}}{c}\right)^2+1+\left(\frac{\hat{B}_\phi}{\hat{B}^{\rm p}}\right)^2-\left(\frac{v_{\rm H}^{\phi}}{c}\right)^2\right], \end{aligned} \tag{94}$$

where $\mathbf{v}_{\rm H}\equiv c\boldsymbol{\beta}$ and $\hat{B}^{\rm p}\equiv|\hat{\mathbf{B}}^{\rm p}|\cdot\hat{B}_r/|\hat{B}_r|$.

The condition for obtaining negative electromagnetic energy-at-infinity $e^{\infty}_{\rm EM}<0$, then, is

$$\left|\frac{\hat{v}^{\phi}_{\rm F}+v^{\phi}_{\rm H}}{c}\right|<\sqrt{\left(\frac{v^{\phi}_{\rm H}}{c}\right)^2-1-\left(\frac{\hat{B}_{\phi}}{\hat{B}^{\rm P}}\right)^2}. \tag{95}$$

Using the relation, $v^{\phi}_{\rm H}=h_{\phi}\omega_{\phi}/\alpha$, this condition becomes

$$|\Omega_{\rm F}|<\frac{\alpha|v^{\phi}_{\rm H}|}{h_{\phi}}\sqrt{1-\left(\frac{c}{v^{\phi}_{\rm H}}\right)^2-\left(\frac{c\hat{B}_{\phi}}{v^{\phi}_{\rm H}\hat{B}^{\rm P}}\right)^2}. \tag{96}$$

Outside the ergosphere, the electromagnetic energy-at-infinity is always positive because $|v^{\phi}_{\rm H}|<c$. In the steady state case, if the rotational energy of the black hole is extracted electromagnetically, the energy-at-infinity at the horizon should be negative. And, if the energy-at-infinity at the horizon is negative, a negative energy-at-infinity region must exist around the black hole because of the continuity of the variables ($\alpha|v^{\phi}_{\rm H}|$, h_{ϕ}, $c/v^{\phi}_{\rm H}$, and $c\hat{B}_{\phi}/v^{\phi}_{\rm H}\hat{B}^{\rm P}$) at $r\geqslant r_{\rm H}$. Therefore, we can demonstrate the existence of a negative energy falling region in the Blandford-Znajek mechanism by evaluating the electromagnetic energy-at-infinity at the horizon. The magnetic field boundary condition at the horizon (Eq. 3.15 of [8]) yields

$$\frac{c}{v^{\phi}_{\rm H}}\frac{\hat{B}_{\phi}}{\hat{B}^{\rm P}}=\frac{\Omega_{\rm F}-\Omega_{\rm H}}{\Omega_{\rm H}}, \tag{97}$$

where $\Omega_{\rm H}\equiv\omega_{\phi}(r_{\rm H})=a/2r_{\rm H}$ is the angular velocity of the black hole horizon. Then condition (96) at the horizon is

$$|\Omega_{\rm F}|<\sqrt{\Omega_{\rm F}(2\Omega_{\rm H}-\Omega_{\rm F})}. \tag{98}$$

Here, we use $|v^{\phi}_{\rm H}|\to\infty$ when $r\to r_{\rm H}$. This condition is identical to $\Omega_{\rm F}<\Omega_{\rm H}$, which is an assumption implicit in the Blandford-Znajek mechanism. Therefore, a region of negative electromagnetic energy-at-infinity exists in the Blandford-Znajek process.

In the Blandford-Znajek process, negative electromagnetic energy-at-infinity plays an important role in extracting the rotational energy of a black hole at the horizon in a causal manner. In fact, we believe that the condition that negative electromagnetic energy-at-infinity exists, Eq. (96), is the same as the condition that the Blandford-Znajek mechanism is operating. We propose to define strictly the Blandford-Znajek mechanism as that black hole energy extraction process that occurs by means of negative *electromagnetic* energy-at-infinity. And, correspondingly, we define the MHD Penrose process, as the extraction process that operates via negative *hydrodynamic* energy-at-infinity. According to our definitions, the both processes are found in the present simulation (Fig. 4 and Fig. 5). The contribution of the MHD Penrose process and the Blandford-Znajek mechanism, respectively, can be evaluated from the hydrodynamic and electromagnetic power radiation, $L^{\rm H}_{\rm hyd}$ and $L^{\rm H}_{\rm EM}$, very near the horizon. We evaluate these powers on a surface $r=0.6r_{\rm S}$, $0.2\pi<\theta<0.8\pi$ and find that they are comparable at $t=6.53\tau_{\rm S}$; $L^{\rm H}_{\rm hyd}/L^{\rm H}_{\rm EM}=1.3$. However, the present simulation has not yet reached a steady state, so such a ratio should be investigated more fully with the longer-term simulations.

In the present simulation, we find energy transport out of the ergosphere, but no outflow of plasma. We believe that this is due to the open magnetic field lines. Energy from the ergosphere is transported outwardly and smoothly along the open field lines before it is converted to kinetic energy of plasma outflow. If we consider closed magnetic field lines across the ergosphere, the energy from the ergosphere will be stored in closed magnetic flux tubes. The magnetic pressure of these flux tubes will increase, elongating the tubes vertically (in the direction of the z-axis), and the plasma confined in the magnetic tube will be accelerated outward. The outflow will be pinched by the magnetic tension, and this pinched plasma flow will become a relativistic jet.

At late times, the elongated magnetic flux tubes will produce an anti-parallel magnetic field near the ergosphere. In this configuration, the electric resistivity will be important. If the resistivity is small but finite (non-zero), magnetic reconnection will occur and release magnetic energy explosively, accelerating the plasma quickly. The accelerated plasma outflow will be directed vertically and become a relativistic jet. Closed magnetic field lines in the ergosphere will be produced by a current ring in the vicinity of the black hole or by charge on the rotating black hole itself (a Kerr-Newman black hole). In extreme dynamical events, such as a failed supernova, the newly-formed black hole may have its own electric charge. Relativistic jets in gamma-ray bursts may be produced by such dynamical processes around Kerr-Newman black holes. However, in this case, the self-gravity of the plasma around the black hole will be significant. (On the other hand, disk self-gravity in AGN is usually negligible.) GRMHD simulations that include self-gravity will be an important tool for investigating relativistic numerical astronomy.

V. SUMMARY

In this paper, we presented the complete numerical method of GRMHD in Kerr space-time. We have applied our GRMHD code to investigate the basic mechanism of the energy extraction from a Kerr black hole by a magnetic field, in particular the simple system of a large-scale magnetic field and thin plasma surrounding a Kerr black hole. Our numerical results show that the rotational energy of the Kerr black hole can be extracted when the magnetic field is strong enough. The extracted energy is transported outward from the ergosphere in a torsional Alfven wave. The electromagnetic power in this Alfven wave is almost the same as that produced by the Blandford-Znajek mechanism [8]: $L_{\rm EM}=(\pi/4)a^2B_0^2r_{\rm H}^2c/\mu_0$. [Note that the expression $L_{\rm EM}=(\pi/4)\times(a^2c/v_{\rm A})B_0^2r_{\rm H}^2c/\mu_0$ is more appropriate when the Alfven velocity is small compared with the speed of light.] We call our mechanism the MHD Penrose process, because the negative energy-at-infinity plays an essential role just like Penrose process. The difference between the classical Penrose process and this one is just the force of the redistribution of the angular momentum. The Penrose process uses particle fission (interaction), while the present mechanism uses magnetic

tension. We also discussed the relation between the MHD Penrose process and the Blandford-Znajek mechanism. The latter can be defined as the black hole rotational energy extraction mechanism that employs negative *electromagnetic* energy-at-infinity, while the MHD Penrose process is defined as one that employs negative *hydrodynamic* energy-at-infinity. In the present numerical simulation, the both mechanisms make roughly equal contributions to the energy extraction. When we consider the extremely strong magnetic field (or small plasma inertia) case, the Alfven surface occurs at the horizon, and the Alfven wave region occupies the entire region just outside of the horizon. The steady state of this case is identical to the force-free solution of [8].

ACKNOWLEDGMENTS

We thank Kazunari Shibata, Takahiro Kudoh, David L. Meier, and Mika Koide for their crucial help for this study. D. L. Meier spent considerable effort checking our manuscript. We appreciate his important comments and suggestions. We appreciate the support of the National Institute for Fusion Science in the use of its supercomputers. This work was supported in part by the Scientific Research Fund of the Japanese Ministry of Education, Culture, Sports, Science, and Technology and Research and Development for Applied Advanced Computational Science and Technology, the Japan Science and Technology Corporation.

APPENDIX: TRANSPORT EQUATIONS AROUND KERR BLACK HOLE

This appendix presents the equations of energy and angular momentum conservation near a Kerr black hole. The Killing vectors for Kerr geometry are $\chi^\nu=(-1,0,0,0)$ and $\eta^\nu=(0,0,0,1)$. In general, any Killing vector ξ^ν has an associated conservation law

$$\frac{1}{\sqrt{-\|g\|}}\frac{\partial}{\partial x^\mu}(\sqrt{-\|g\|}T^{\mu\nu}\xi_\nu)=0. \tag{A1}$$

Using $\|g\|=-(\alpha h_1 h_2 h_3)^2$, this equation becomes

$$\frac{\partial}{\partial t}(\alpha T^{0\nu}\xi_\nu)=-\frac{1}{h_1 h_2 h_3}\sum_i \frac{\partial}{\partial x^i}(\alpha h_1 h_2 h_3 c T^{i\nu}\xi_\nu). \tag{A2}$$

For the Killing vector χ^ν, the law of energy conservation becomes

$$\frac{\partial e^\infty}{\partial t}=-\hat{\nabla}\cdot\mathbf{S}, \tag{A3}$$

where $e^\infty\equiv\alpha T^{0\nu}\xi_\nu$ is called *energy-at-infinity* density and $S^i\equiv c\alpha h_i T^{i\nu}\xi_\nu$ is energy flux density. Here we also express these quantities in the FIDO frame as

$$e^\infty=\alpha(\epsilon+Dc^2)+\sum_i \omega_i h_i \hat{P}^i, \tag{A4}$$

$$S^i=\alpha\left[\alpha c^2\hat{P}^i+e^\infty c\beta^i+\sum_j \alpha c\beta^j\hat{T}^{ij}\right]. \tag{A5}$$

Note that the energy-at-infinity must be positive everywhere except in the ergosphere. These quantities can be divided into components as follows:

$$e^\infty=e^\infty_{\rm hyd}+e^\infty_{\rm EM}, \tag{A6}$$

$$S^i=S^i_{\rm hyd}+S^i_{\rm EM}, \tag{A7}$$

where

$$e^\infty_{\rm hyd}=\alpha(\mathfrak{h}\gamma^2-p)+\sum_i \omega_i h_i\frac{\mathfrak{h}}{c^2}\gamma^2\hat{v}^i, \tag{A8}$$

$$e^\infty_{\rm EM}=\alpha\left(\frac{\hat{B}^2}{2}+\frac{\hat{E}^2}{2c^2}\right)+\sum_i \omega_i h_i\frac{1}{c^2}(\hat{\mathbf{E}}\times\hat{\mathbf{B}})_i, \tag{A9}$$

$$S^i_{\rm hyd}=\alpha^2\mathfrak{h}\gamma^2\left(1+\sum_j \frac{c\beta^j\hat{v}^j}{c^2}\right)(\hat{v}^i+c\beta^i), \tag{A10}$$

$$S^i_{\rm EM}=\alpha^2\left[(\hat{\mathbf{E}}-c\boldsymbol{\beta}\times\hat{\mathbf{B}})\times\left(\hat{\mathbf{B}}+c\boldsymbol{\beta}\times\frac{\hat{\mathbf{E}}}{c^2}\right)\right]^i, \tag{A11}$$

where the subscripts ''hyd'' and ''EM'' indicate hydrodynamic and electromagnetic components, respectively.

For the Killing vector η^ν, we have the equation of angular momentum conservation

$$\frac{\partial l}{\partial t}=-\hat{\nabla}\cdot\mathbf{M}, \tag{A12}$$

where $l\equiv\alpha T^{0\nu}\eta_\nu/c$ and $M^i\equiv\alpha h_i T^{i\nu}\eta_\nu$ are the angular momentum density and the angular momentum flux density, respectively. Using the quantities measured in the FIDO frame, we write

$$l=h_3\hat{P}^3, \tag{A13}$$

and

$$M^i=\alpha h_3(\hat{T}^{i3}+c\beta^i\hat{P}^3). \tag{A14}$$

These variables also can be divided into hydrodynamic and electromagnetic components, denoted by the subscripts ''hyd'' and ''EM,'' as follows:

$$l=l_{\rm hyd}+l_{\rm EM}, \tag{A15}$$

$$M^i=M^i_{\rm hyd}+M^i_{\rm EM}, \tag{A16}$$

where

$$l_{\rm hyd}=h_3\frac{\mathfrak{h}}{c^2}\gamma^2\hat{v}^3, \tag{A17}$$

$$l_{\rm EM}=\frac{h_3}{c^2}(\hat{\mathbf{E}}\times\hat{\mathbf{B}})_3, \tag{A18}$$

$$M^i_{\rm hyd}=\alpha h_3\left[p\,\delta^{i3}+\frac{\hbar}{c^2}\gamma^2\hat{v}^i\hat{v}^3+c\beta^i\frac{\hbar}{c^2}\gamma^2\hat{v}^3\right], \tag{A19}$$

$$M^i_{\rm EM}=\alpha h_3\left[\left(\frac{\hat{B}^2}{2}+\frac{\hat{E}^2}{2c^2}\right)\delta^{i3}-\hat{B}_i\hat{B}_3-\frac{\hat{E}_i\hat{E}_3}{c^2}+\frac{c\beta^i}{c^2}(\hat{\mathbf{E}}\times\hat{\mathbf{B}})_3\right]. \tag{A20}$$

We can see that the hydrodynamic energy-at-infinity and angular momentum densities (A8) and (A17) are similar to those for a particle with the mass m,

$$E^\infty=\alpha mc^2\gamma+\omega_3 h_3 m\gamma\hat{v}^\phi, \tag{A21}$$

$$L=h_3 m\gamma\hat{v}^\phi, \tag{A22}$$

respectively [35]. Furthermore, noting that $(\hat{B}^2/2+\hat{E}^2/2c^2)/c^2$ and $\hat{\mathbf{E}}\times\hat{\mathbf{B}}/c^2$ correspond to the effective electromagnetic mass and momentum densities in the FIDO frame, we also find a similarity between the electromagnetic energy-at-infinity and angular momenta [Eqs. (A9) and (A18)] and those of one particle [Eqs. (A21) and (A22)].

Next we present the transport equations of electromagnetic energy and momentum near a Kerr black hole. The general relativistic Maxwell equations (75)–(78) yield

$$\frac{\partial e^\infty_{\rm EM}}{\partial t}=-\hat{\nabla}\cdot\mathbf{S}_{\rm EM}-\alpha(\hat{\mathbf{v}}+c\boldsymbol{\beta})\cdot\mathbf{f}_{\rm L}, \tag{A23}$$

$$\frac{\partial l_{\rm EM}}{\partial t}=-\hat{\nabla}\cdot\mathbf{M}_{\rm EM}-h_3 f^3_{\rm L}, \tag{A24}$$

where $\mathbf{f}_{\rm L}=\rho_e\hat{\mathbf{E}}+\hat{\mathbf{J}}\times\hat{\mathbf{B}}$ is the Lorentz force density. Subtracting the both sides of the electromagnetic transport equations (A23) and (A24) from the conservation equations (A3) and (A12), respectively, we derive the hydrodynamic transport equations of energy and angular momentum

$$\frac{\partial e^\infty_{\rm hyd}}{\partial t}=-\hat{\nabla}\cdot\mathbf{S}_{\rm hyd}+\alpha(\hat{\mathbf{v}}+c\boldsymbol{\beta})\cdot\mathbf{f}_{\rm L}, \tag{A25}$$

$$\frac{\partial l_{\rm hyd}}{\partial t}=-\hat{\nabla}\cdot\mathbf{M}_{\rm hyd}+h_3 f^3_{\rm L}. \tag{A26}$$

When we replace the suffixes ''hyd'' and ''EM'' by ''+'' and ''−'' respectively, the transport equation of energy and angular momentum can be summarized as

$$\frac{\partial e^\infty_\pm}{\partial t}=-\hat{\nabla}\cdot\mathbf{S}_\pm\pm\alpha(\hat{\mathbf{v}}+c\boldsymbol{\beta})\cdot\mathbf{f}_{\rm L}, \tag{A27}$$

$$\frac{\partial l_\pm}{\partial t}=-\hat{\nabla}\cdot\mathbf{M}_\pm\pm h_3 f^3_{\rm L}. \tag{A28}$$

[1] J. A. Biretta, W. B. Sparks, and F. Macchetto, Astrophys. J. **520**, 621 (1999).
[2] T. J. Pearson and J. A. Zensus, in *Superluminal Radio Sources*, edited by J. A. Zensus and T. J. Pearson (Cambridge University Press, London, 1987), p. 1.
[3] I. F. Mirabel and L. F. Rodriguez, Nature (London) **374**, 141 (1994).
[4] S. J. Tingay *et al.*, Nature (London) **374**, 141 (1995).
[5] S. R. Kulkarni, Nature (London) **398**, 389 (1999).
[6] K. Makishima *et al.*, Astrophys. J. **535**, 632 (2000).
[7] R. Penrose, Nuovo Cimento **1**, 252 (1969).
[8] R. D. Blandford and R. Znajek, Mon. Not. R. Astron. Soc. **179**, 433 (1977).
[9] B. Punsly and F. V. Coroniti, Astrophys. J. **354**, 583 (1990).
[10] S. Koide, K. Shibata, T. Kudoh, and D. L. Meier, Science (Washington, DC, U.S.) **295**, 1688 (2002), published online 24 January 2002; 10.1126/science.1068240.
[11] S. Weinberg, *Gravitation and Cosmology* (Wiley, New York, 1972).
[12] S. Koide, K. Shibata, and T. Kudoh, Astrophys. J. Lett. **495**, L63 (1998).
[13] S. Koide, K. Shibata, and T. Kudoh, Astrophys. J. **522**, 727 (1999).
[14] S. Koide, D. L. Meier, K. Shibata, and T. Kudoh, Astrophys. J. **536**, 668 (2000).
[15] S. Koide, K. Shibata, T. Kudoh, and D. L. Meier, J. Korean Astron. Soc. **34**, S215 (2001).
[16] S. Koide, K.-I. Nishikawa, and R. L. Mutel, Astrophys. J. Lett. **463**, L71 (1996).
[17] S. Koide, Astrophys. J. **478**, 66 (1997).
[18] K. S. Thorne, R. H. Price, and D. A. Macdonald, *Membrane Paradigm* (Yale University Press, New Haven, 1986).
[19] S. F. Davis, NASA Contractor Rep. 172373 (ICASE Rep. 84-20) (NASA, Washington, DC, 1984).
[20] G. C. Duncan and P. A. Hughes, Astrophys. J. **321**, 334 (1994).
[21] R. M. Wald, Phys. Rev. D **10**, 1680 (1974).
[22] D. L. Meier, Astrophys. J. **522**, 753 (1999).
[23] M. Yokosawa, Publ. Astron. Soc. Jpn. **45**, 207 (1993).
[24] R. D. Blandford and D. Payne, Mon. Not. R. Astron. Soc. **199**, 883 (1982).
[25] Y. Uchida and K. Shibata, Publ. Astron. Soc. Jpn. **37**, 515 (1985).
[26] K. Shibata and Y. Uchida, Publ. Astron. Soc. Jpn. **38**, 631 (1986).
[27] R. Ouyed, R. E. Pudritz, and J. M. Stone, Nature (London) **385**, 409 (1997).
[28] T. Kudoh, R. Matsumoto, and K. Shibata, Astrophys. J. **508**, 186 (1998).
[29] D. L. Meier, S. Koide, and Y. Uchida, Science (Washington, DC, U.S.) **291**, 84 (2001).
[30] J. A. Font, J. M. Ibanez, and P. Papadopoulos, Astrophys. J. Lett. **507**, L67 (1998).
[31] M. Takahashi, S. Nitta, Y. Tatematsu, and A. Tomimatsu, Astrophys. J. **363**, 206 (1990).

[32] K. Hirotani, M. Takahashi, S.-Y. Nitta, and A. Tomimatsu, Astrophys. J. **386**, 455 (1992).
[33] D. L. Meier, Astrophys. J. Lett. **548**, L9 (2001).
[34] Shorthand notation used is as follows: $\nabla_\mu A^\nu = \partial_\mu A^\nu + \Gamma^\nu_{\mu\rho} A^\rho$; $\nabla_\mu (A^\nu B^\lambda) = (\nabla_\mu A^\nu) B^\lambda + A^\nu (\nabla_\mu B^\lambda)$; $\Gamma^\rho_{\mu\rho} = \partial_\mu [\log(-\|g\|)^{1/2}]$.
[35] Here we briefly summarize one particle motion around a Kerr black hole in the equatorial plane. Equations (A21) and (A22) give $E^\infty/mc^2 = \alpha[1+(L/mch_3)^2]^{1/2}/[1-(\hat{v}_r/c)^2]^{1/2} + \omega_3 L/mc^2 \geqslant \alpha[1+(L/mch_3)^2]^{1/2} + \omega_3 L/mc^2 \equiv \Phi(r)$, where the equal in the inequality corresponds to $\hat{v}_r = 0$. The function $c^2\Phi(r)$ is the effective gravitational potential. A circular orbit for a particle occurs when $\partial\Phi/\partial r = 0$. This condition gives the orbital velocity of the particle, i.e. the Kepler velocity, $\tilde{v}^\phi_{\rm K} = cA[\pm(r_{\rm g}/r)^{1/2} - a r_{\rm g}^2/r^2]/\Delta^{1/2}(r^3 - r_{\rm g}^3 a^2)$, where the positive sign corresponds to orbits that corotate with the black hole and the negative sign to counter-rotating orbits. The velocity in the FIDO frame is given by $\hat{v}^\phi_{\rm K} = \tilde{v}^\phi_{\rm K} - c\beta^\phi$. In the Schwarzschild black hole case ($a=0$), the Kepler velocity is simply $\hat{v}_{\rm K} = \pm c/[2(r/r_{\rm S}-1)]^{1/2}$. The particle orbit is unstable when $\partial\Phi/\partial r = 0$ and $\partial^2\Phi/\partial r^2 < 0$ or $\partial L_{\rm K}/\partial r < 0$, where $L_{\rm K}$ is the angular momentum of the particle in the circular orbit, $L_{\rm K} = h_3 m \hat{v}^\phi_{\rm K}/[1-(\hat{v}^\phi_{\rm K}/c)]^{1/2}$. The "last stable orbit" is determined by $\partial L_{\rm K}/\partial r = 0$. For a Schwarzschild black hole the radius of the last stable orbit is $3r_{\rm S}$. For a maximally-rotating Kerr black hole ($a=1$), the radius of the corotating particle orbit is $0.5r_{\rm S} = r_{\rm g} = r_{\rm H}$ and counter-rotating orbit is $4.5r_{\rm S}$.
[36] Note: the velocity of the MHD fast mode is given by $v_{\rm f} = c[(B_0^2 + \Gamma p_0)/(\mathfrak{h}_0 + B_0^2)]^{1/2}$, where $\mathfrak{h}_0 = \rho_0 c^2 + \Gamma p_0/(\Gamma - 1)$ is the relativistic enthalpy density.